Check for updates

Advanced Optical Materials

ADVANCED OPTICAL MATERIALS
www.advopticalmat.de

RESEARCH ARTICLE OPEN ACCESS

Intramolecular Direct Arylation Enables Access to Diverse Photophysical Properties for π-Expanded 1,4-Dihydropyrrolo[3,2-*b*]pyrroles

Damian Kusy[1] | Krzysztof Górski[1] | Carmelo Naim[2] | Francesco Bertocchi[3] | Nicolas Vanthuyne[4] | Krzysztof Noworyta[5] | Bartosz Szymański[6] | Radosław Kamiński[6] | Francesca Terenziani[3] | Denis Jacquemin[2,7] | Daniel T. Gryko[1]

[1]Institute of Organic Chemistry, Polish Academy of Sciences, Warsaw, Poland | [2]Nantes Université, CNRS, CEISAM UMR 6230, Nantes, France | [3]Department of Chemistry, Life Sciences and Environmental Sustainability, University of Parma, Parma, Italy | [4]Aix Marseille Univ, CNRS, Centrale Med, UAR 1739, FSCM, Chiropole, Marseille, France | [5]Institute of Physical Chemistry, Polish Academy of Sciences, Warsaw, Poland | [6]Faculty of Chemistry, Warsaw University, Warsaw, Poland | [7]Institute Universitaire de France (IUF), Paris, France

Correspondence: Francesca Terenziani (francesca.terenziani@unipr.it) | Denis Jacquemin (denis.jacquemin@univ-nantes.fr) | Daniel T. Gryko (dtgryko@icho.edu.pl)

Received: 9 August 2026 | **Revised:** 17 September 2026 | **Accepted:** 22 September 2026

Keywords: aromaticity | conjugated system | enantiomer | luminescence | molecular symmetry | solvatochromism

ABSTRACT

Dyes incorporating 1,4-dihydropyrrolo[*3,2-b*]pyrrole (DHPP) units are attractive platforms for organic optoelectronics because of their tunable electronic structures and intense fluorescence. Herein, we report a modular synthetic route to a diverse family of π-expanded DHPPs. The approach relies on double intramolecular direct arylation. This strategy provides efficient access to structurally complex dyes, including helically twisted and highly fused π-systems containing up to 20 conjugated aromatic rings and a unique combination of optical properties. Several of the obtained dyes display pronounced solvatochromism, red emission, and circularly polarized luminescence (CPL). In particular, chiral resolution of a helicene-type derivative enabled detailed chiroptical studies and revealed configurationally stable enantiomers with a good luminescence dissymmetry factor. A combination of experimental and computational analyses provided insight into the structure–property relationships governing their photophysical behavior, with particular emphasis on molecular symmetry and the substituent-dependent influence of nitro groups.

1 | Introduction

Nitrogen-doped nanographenes have emerged as a promising class of π-conjugated materials owing to their unique combination of tunable electronic properties, enhanced chemical reactivity, and improved charge carrier mobility [1–15]. The incorporation of nitrogen atoms into polycyclic aromatic frameworks induces local perturbations in the electronic structure and enables the precise modulation of molecular orbital energies, which can be particularly advantageous for applications in organic electronics, photovoltaics, catalysis, and bioimaging. Among the various classes of these molecular architectures, functional dyes based of pyrrole skeleton have attracted the strongest attention recently (Figure 1) [16–19]. The inherent reactivity of pyrrole and its π-expanded analogs, as well as the attractive physicochemical and optoelectronic properties of the resulting molecular nanographenes, are responsible for this trend [12, 20–24]. In this context, the 1,4-dihydropyrrolo[3,2-*b*]pyrrole (DHPP) scaffold has attracted considerable attention as a privileged structural motif. Its rigid, centrosymmetric, and

This is an open access article under the terms of the Creative Commons Attribution License, which permits use, distribution and reproduction in any medium, provided the original work is properly cited.
© 2026 The Author(s). *Advanced Optical Materials* published by Wiley-VCH GmbH

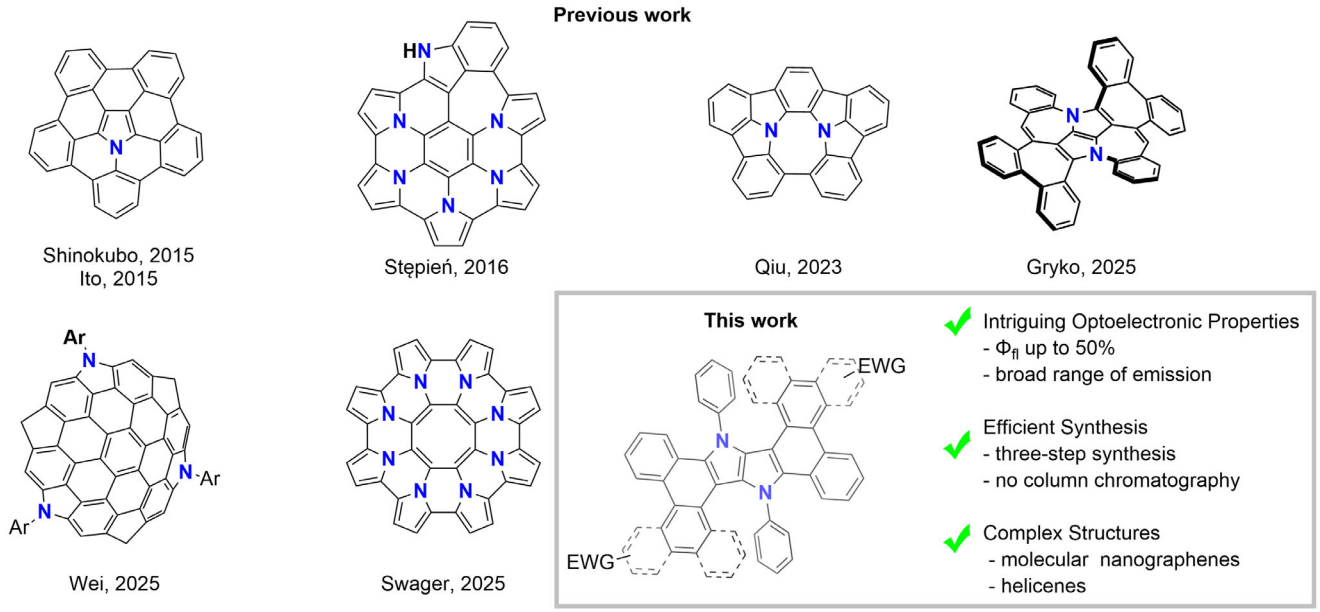


FIGURE 1 | Chemical structures of exemplary pyrrole-based N-doped nanographenes.

electron-rich architecture promotes effective π-conjugation and offers multiple sites for functionalization, making it ideally suited for the bottom-up construction of π-extended systems [25–28].

Recent studies have demonstrated that π-expanded DHPPs exhibit outstanding photophysical characteristics, including strong absorption in the visible and near-infrared regions, as well as high fluorescence quantum yields. These features, combined with their ability to engage in both donor–acceptor interactions and supramolecular assembly, render them attractive candidates for applications in organic field-effect transistors (OFETs), organic light-emitting diodes (OLEDs) [29, 30], organic solar cells, and fluorescent probes [31]. In addition, DHPP derivatives have been explored as building blocks for thermally activated delayed fluorescence (TADF) and aggregation-induced-emission-active systems [32]. DHPPs have recently been highlighted as simple, tailorable building blocks for conjugated polymers with potential in optoelectronic and electrochromic applications [33].

The predominant strategy for the synthesis of π-expanded DHPPs relies on the Scholl reaction, which is limited to electron-rich and electron-neutral systems [34]. Moreover, steric congestion around the reactive sites can redirect the expected six-membered-ring closure toward the formation of five-membered spirocyclic products [35]. Representative examples include butterfly-shaped π-systems [36], bowl-shaped [37], and saddle-shaped nanographenes [38]. An alternative strategy exploits 2-bromophenyl substituents at the 1,2,4 and 5 positions as synthetic handles for intramolecular direct arylation [39, 40]. However, a key drawback of this approach is the difficulty associated with preparation of the required TAPP precursors, particularly from 2-haloanilines.

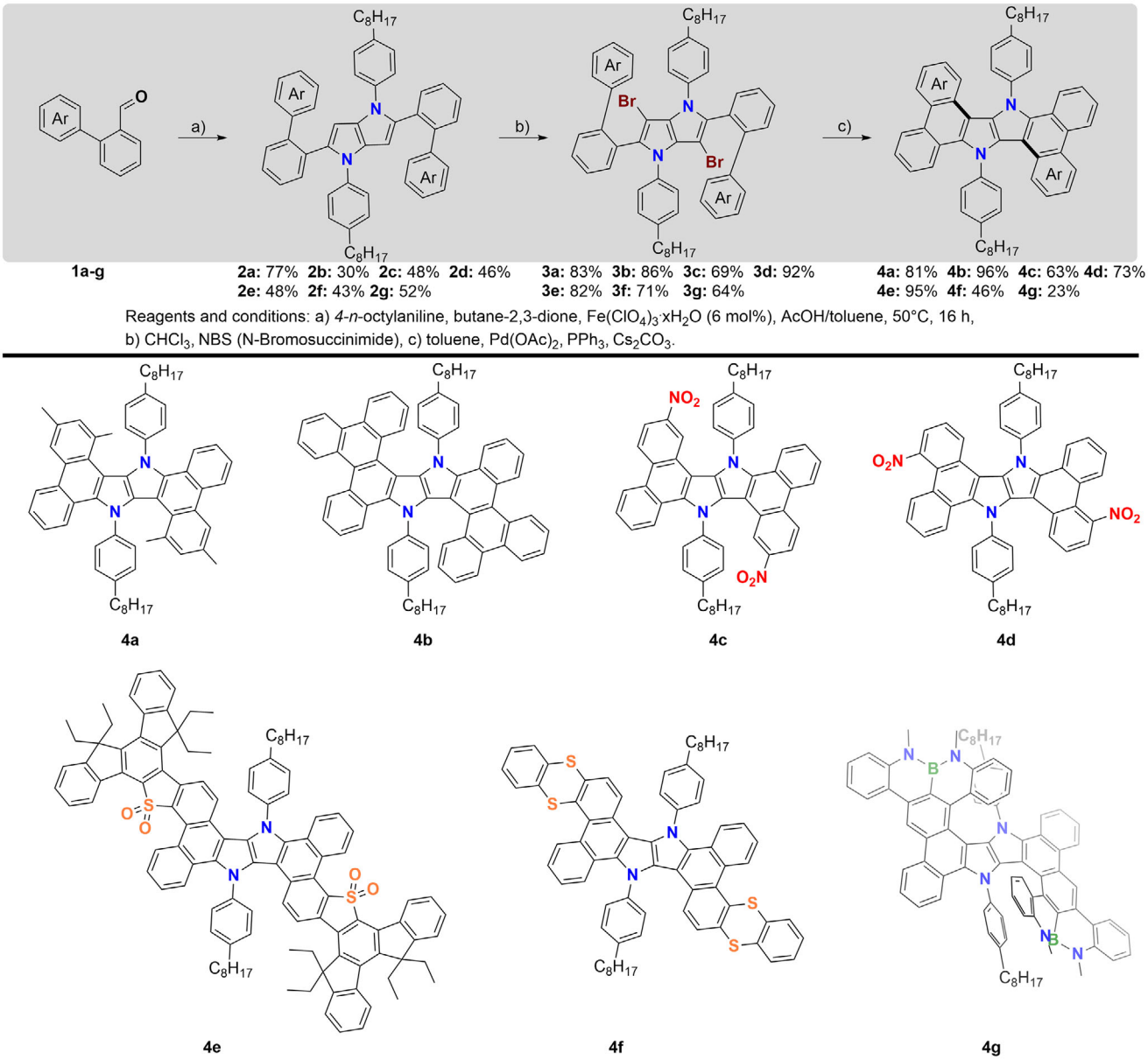
A complementary strategy based on photoinduced 6π-electrocyclization has also been developed [41]. This method enabled the synthesis of the first stable DHPP-based double helicenes [42]. Although this approach offers high regioselectivity, which arises from the intrinsic nature of the 6π-electrocyclization process, it is strongly governed by the symmetry of the excited-state wavefunction and the distribution of LUMO electron density. Consequently, the outcome of photocyclization is highly dependent on the steric hindrance [43], the substitution pattern, and the electronic character of the substituent.

Thus, despite significant progress, the synthesis of structurally diverse and functionally relevant π-expanded DHPPs remains challenging. The limitations of existing methodologies prompted us to develop a more general approach applicable irrespective of steric hindrance and electronic structure. Herein, we present a complementary protocol for the annulation of DHPP derivatives in which Pd-catalyzed intramolecular direct arylation is the key step. The key advantage of this new approach is that it is applicable for substrates in which LUMO electron density is predominantly localized at the acceptor moiety and which undergo complete decomposition under conventional 6π-electrocyclization conditions and Scholl reaction conditions. Moreover, Pd-catalyzed intramolecular direct arylation enables the use of derivatives bearing not only electron-withdrawing groups but also sterically demanding substituents [44].

2 | Results and Discussion

Our envisioned synthetic concept relies on the preparation of tetraarylpyrrolo[3,2-*b*]pyrroles (TAPPs) from sterically congested aldehydes, followed by double bromination of DHPP core at 3- and 6- positions and subsequent double intramolecular direct arylation. Both bromination and intramolecular direct arylation were expected to proceed irrespective of the electronic and steric properties of the substituents attached to the DHPP core. Our synthetic route toward π-expanded π-expanded DHPPs commenced with the preparation of aldehydes **1a**–**1g** via Suzuki–Miyaura cross-coupling reactions. These aldehydes bear a diverse range of electron-rich and electron-deficient aromatic substituents at

21951071, 2026, 39, Downloaded from https://advanced.onlinelibrary.wiley.com/doi/10.1002/adom.71894 by Francesca Terenziani - University Degli Studi Di Parma Stampa Universitaria Parmense , Wiley Online Library on [26/10/2026]. See the Terms and Conditions (https://onlinelibrary.wiley.com/terms-and-conditions) on Wiley Online Library for rules of use; OA articles are governed by the applicable Creative Commons License



SCHEME 1 | Synthesis and chemical structures of π-expanded DHPPs **4a**–**4g**.

the *ortho* position. The resulting substrates were subsequently converted into TAPPs **2a**–**2g** through a one-pot condensation with aromatic amines [45], affording the desired products in good to very good yields (43-77%). Selective bromination of the DHPP core with N-bromosuccinimide (NBS) afforded the corresponding dibrominated intermediates **3a**–**3g** in 64–92% yields (Scheme 1).

The final step involved double intramolecular direct arylation to construct fully fused π-expanded DHPPs **4a-g**. To ensure both practicality and broad applicability, a readily available catalytic system comprising palladium(II) acetate, triphenylphosphine, and caesium carbonate in toluene was employed. Most reactions proceeded to completion with quantitative substrate conversion, even when electron-deficient arenes acted as the nucleophilic coupling partners, as exemplified by compounds **4c**–**4e**. Among the synthesized N-doped molecular π-expanded DHPPs, dye **4e** is particularly noteworthy. It contains two 5-thiatruxene units, resulting in a molecule with 20 fused aromatic rings and a molecular mass of 1638 Da. Despite its considerable steric congestion, compound **4e** was obtained in an excellent yield of 95%. Another particularly challenging target was π-expanded DHPP **4g**, featuring a doubly helically twisted scaffold incorporating two B, N-doped six-membered rings. Despite the pronounced steric congestion associated with the final ring-closing events, the developed protocol enabled the formation of the fully fused product in 23% yield. The reduced efficiency observed for this exceptionally demanding substrate was attributed to competing monoarylation and dehalogenation pathways.

Compound **4g** was obtained as a mixture of two enantiomers (the meso-form has not formed). Enantiomeric separation was achieved by chiral HPLC using a Whelk-O1 column, and the isolated species were characterized by circular dichroism (CD) spectroscopy, optical rotation measurements, and circularly polarized luminescence (CPL) spectroscopy. These analyses revealed distinct chiroptical signatures and confirmed the configurational

21951071, 2026, 39, Downloaded from https://advanced.onlinelibrary.wiley.com/doi/10.1002/adom.71894 by Francesca Terenziani - University Degli Studi Di Parma Stampa Universitaria Parmense , Wiley Online Library on [26/10/2026]. See the Terms and Conditions (https://onlinelibrary.wiley.com/terms-and-conditions) on Wiley Online Library for rules of use; OA articles are governed by the applicable Creative Commons License

TABLE 1 | Spectroscopic data in hexane (green), toluene (black), dichloromethane (red), tetrahydrofuran (orange), dimethylformamide (blue), and in solid for compounds **4a**-**4g**.

Dye	λ_{abs} [nm] (ε [10^3 cm^{-1} M^{-1}])	λ_{fl} [nm]	$\Delta\nu$ [cm^{-1}]	Φ_{fl} [%]	λ_{fl}^{SOLID} [nm]	Φ_{fl}^{SOLID} [%]
4a	391 (47.9), 414 (38.8)	436	1220	52	460	10.2
	387 (46.2), 408 (37.2)	446	2090	46		
	384 (45.6), 405 (37.3)	454	2660	58		
4b	349 (70.9), 429 (7.4)	462	1670	29	499	4.2
	348 (83.6), 427 (7.6)	480	2590	27		
	345 (82.9), 425 (7.4)	482	2780	31		
4c	351 (34.3), 455 (7.5), 483 (5.6)	517	1360	21.0	593	9.5
	357 (47.9), 467 (9.5)	623	5360	7.8		
	353 (48.5), 463 (9.4)	672	6720	2.9		
	355 (48.7), 467 (9.0)	833	9410	<0.001		
4d	374 (27.9), 465 (9.6)	603	4920	0.2	n.d.	n.d.
	343 (45.1), 414 (12.2)	677	9380	2.4		
	340 (45.9), 414 (12.3)	734	10530	0.4		
	345 (46.3), 414 (12.2)	841	12260	<0.001		
	344 (44.3), 413 (12.0)	n.d.	n.d.	n.d.		
4e	374 (39.4), 418 (11.3)	508	4240	15	614	0.6
	378 (59.7), 410 (20.6)	530	5520	21		
	377 (47.3), 414 (15.7)	564	6420	20		
	378 (47.4), 412 (17.8)	598	7550	23		
	379 (41.2), 414 (15.7)	622	8080	16		
4f	388 (27.8), 414 (21.2)	435	1170	3.9	n.d.	n.d.
	385 (31.8), 412 (22.1)	461	2580	3.1		
	386 (33.9), 413 (23.6)	472	3030	4.5		
	385 (30.0), 413 (20.1)	473	3070	5.2		
4g	396 (46.8), 448 (18.3)	464	770	27	n.d.	n.d.
	402 (54.1), 451 (23.0)	469	850	38		
	404 (51.4), 450 (23.0)	476	1210	31		
	404 (49.1), 451 (23.0)	473	1030	39		

[a] λ_{abs} / λ_{fl} – absorption / emission wavelength, ε – molar absorption coefficient, $\Delta\nu$ – Stokes shift, Φ_{fl} – fluorescence quantum yield in solution, λ_{fl}^{SOLID} – emission wavelength, Φ_{fl}^{SOLID} fluorescence quantum yield in solid

stability of the helical structures. Importantly, neither the TAPP formation nor the bromination steps required chromatographic purification, because all intermediates precipitated cleanly from methanol. This synthetic efficiency, combined with the robustness of the key direct arylation step, renders the method scalable and well suited to the gram-scale preparation of structurally diverse functional π-systems.

2.1 | Photophysical Properties

The described intramolecular direct arylation protocol offers a straightforward approach to tuning photophysical properties. Fusion of the peripheral oligoaryl subunits with the central 1,4-dihydropyrrolo[3,2-*b*]pyrrole core significantly expands and rigidifies the π-electron system. As a result, bathochromic shifts of both absorption (λ_{abs} = 414 nm) and emission (λ_{fl} = 436 nm) are observed, while good emissive properties are retained ($\Phi_{fl} \approx$ 50%) for **4a** (Table 1). These features resemble those of previously reported DHPP-based functional dyes [34, 36, 45]. Replacement of the benzene ring with a phenanthrene unit in dye **4b** or a thianthrene moiety in product **4f** slightly affects the absorption maxima (Table 1), indicating that the applied π-expansion strategy modulates the optical bandgap of the chromophore. Nevertheless, a more pronounced effect is observed for the molar absorption coefficient (ε). In both cases, the most red-shifted absorption bands show a noticeable decrease in ε; however, for **4b** this decrease is particularly large, by approximately a factor of five compared with **4a** (Table 1). π-Expansion also affects both the fluorescence spectra and fluorescence quantum yields.

The centrosymmetric dyes **4b** and **4f** exhibit weak solvatochromic behavior in emission (Figures S39 and S46), suggesting excited-state symmetry breaking [46, 47]; however, this effect remains modest, likely because of the absence of a strong electron-accepting substituent. In contrast, the distortion of molecule **4b**, caused by steric repulsion between the phenanthrene scaffold and the adjacent benzene ring, enhances non-radiative deactivation of the excited state, leading to a decrease in fluorescence quantum yield to $\Phi_{fl} \approx$ 30%. However, the even larger decrease in Φ_{fl} observed for dye **4f** (Table 1) cannot be attributed solely to steric effects. We hypothesize that the presence of four sulfur atoms promotes intersystem crossing (ISC), thereby opening an efficient

21951071, 2026, 39, Downloaded from https://advanced.onlinelibrary.wiley.com/doi/10.1002/adom.71894 by Francesca Terenziani - University Degli Studi Di Parma Stampa Universitaria Parmense , Wiley Online Library on [26/10/2026]. See the Terms and Conditions (https://onlinelibrary.wiley.com/terms-and-conditions) on Wiley Online Library for rules of use; OA articles are governed by the applicable Creative Commons License

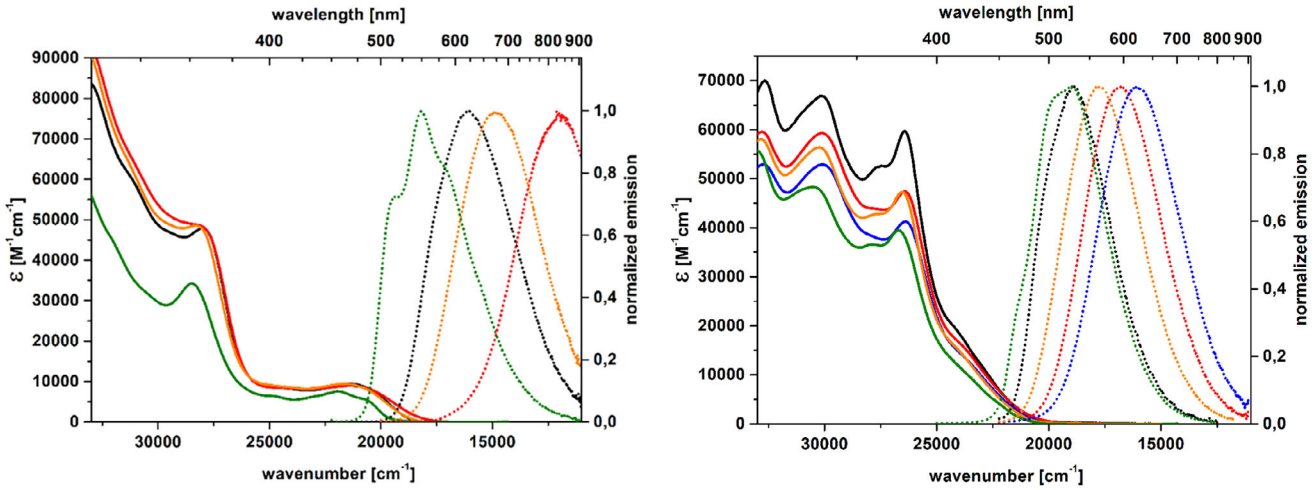


FIGURE 2 | Absorption (solid) and emission (dot) spectra of 4c (left) and 4e (right) in hexane, toluene, tetrahydrofuran, dichloromethane and dimethylformamide.

non-radiative deactivation pathway through the T_1 excited state [48].

The observation of fluorescence in the crystalline state for dye **4a** prompted us to investigate this phenomenon systematically. Upon going from solution to the solid state, a bathochromic shift of the fluorescence spectrum is observed, accompanied by a significant decrease in emission quantum yield for **4a** and **4b**. In contrast, no solid-state emission could be detected for **4f** (Table 1), suggesting substantial aggregation-caused fluorescence quenching.

Peripheral decoration of the electron-rich 1,4-dihydropyrrolo[3,2-*b*]pyrrole core with electron-withdrawing units, such as the NO_2 group (**4c**,**d**) or 5-thiatruxene sulfone (**4e**), leads to quadrupolar donor–acceptor (D–A) systems with valuable solvatochromic properties. Compared to the compounds discussed above, dyes **4c**–**e** exhibit noticeably red-shifted absorption spectra, with λ_{abs} up to 483 nm for dye **4c** (Figure 2), and lower ε values than compound **4a**. The changes in the absorption spectra upon varying solvent polarity remain limited, which is consistent with the nearly centrosymmetric nature of dyes **4c**–**e** (Figure 2). The impact of the electron-deficient unit is, however, much more pronounced in emission. As is typical for charge-transfer transitions, broad fluorescence spectra are observed, with a strong bathochromic shift upon increasing solvent polarity, reaching the near-infrared region (λ_{fl} = 841 nm) for **4d** in dichloromethane, accompanied by a very large Stokes shift ($\Delta\nu$ = 12260 cm^{-1}) (Table 1, Figure S43). Unfortunately, in contrast to other nitroaromatics bearing a DHPP core [47], Φ_{fl} values for **4c**,**d** are significantly decreased, most likely as a result of the combined effects of internal conversion and intersystem crossing [29, 48–50]. Due to the weaker electron-accepting properties of the SO_2 group in dye **4e** compared with the NO_2 group, charge separation in the S_1 state of dye **4e** remains moderate, and the fate of the excited state is less affected by the so-called energy gap law [50, 51]; $\Phi_{fl} \approx 20\%$ in all investigated solvents (Table 1). Once again, going from solution to the solid state results in a decrease in emission quantum yield, accompanied by a bathochromic shift to the orange-red region for **4c** and **4e**, whereas **4d** does not exhibit significant solid-state emission (Table 1).

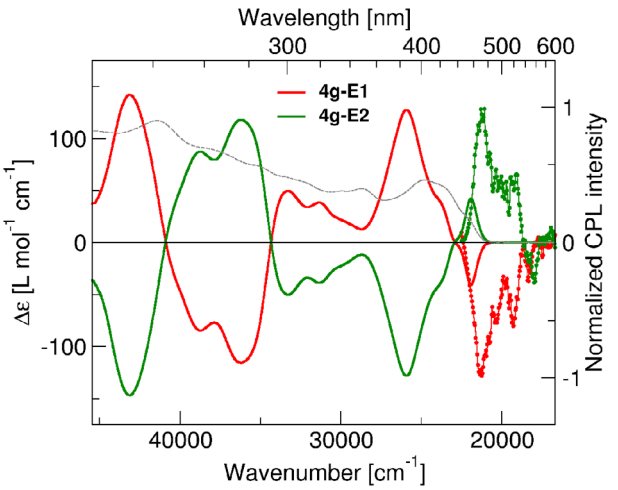


FIGURE 3 | CD (full lines) and CPL (thin lines with dots) spectra of the enantiomers of **4g** in dichloromethane. Grey line: absorption spectrum (arbitrary units).

2.2 | Chiroptical Properties

The circular dichroism (CD) spectra of the separated enantiomers of **4g** in dichloromethane (Figure 3) exhibit multiple bands, with absorption dissymmetry factors (g_{abs}) remaining well below 10^{-2}. Circularly polarized luminescence (CPL) spectra of the **4g** enantiomers in dichloromethane were recorded upon excitation at 405 nm. To minimize possible artifacts arising from linearly polarized emission components, a horizontal polarizer was placed in the excitation path [51, 52]. As shown in Figure 3, the CPL spectra closely resemble the fluorescence spectra recorded in the same solvent (Figure S47), displaying comparable band shapes and weak indications of vibronic progression. The luminescence dissymmetry factor (g_{lum}) is approximately 2.2×10^{-3}, which is

21951071, 2026, 39, Downloaded from https://advanced.onlinelibrary.wiley.com/doi/10.1002/adom.71894 by Francesca Terenziani - University Degli Studi Di Parma Stampa Universitaria Parmense , Wiley Online Library on [26/10/2026]. See the Terms and Conditions (https://onlinelibrary.wiley.com/terms-and-conditions) on Wiley Online Library for rules of use; OA articles are governed by the applicable Creative Commons License

TABLE 2 | Chiroptical properties of **4g** in hexane (green) and dichloromethane (red).

g_{lum} (E1/E2)	Φ_{fl}	ε_{400nm} [$M^{-1}\cdot cm^{-1}$]	B_{CPL} [M^{-1} cm^{-1}]
$-2.05\cdot10^{-3}$/ $1.96\cdot10^{-3}$	0.27	$4.6\cdot10^{4}$	12.5
$-2.25\cdot10^{-3}$/ $2.19\cdot10^{-3}$	0.31	$5\cdot10^{4}$	17.2

g_{lum} – fluorescence dissymmetry factor, Φ_{fl} – fluorescence quantum yield, ε_{400nm} – absorption coefficient, B_{CPL} – CPL brightness

in line with values reported for other helicenes containing B—N bonds [52, 53] and indicates moderate chiral emission activity. This value is very similar to the g_{abs} value of the lowest-energy CD band, approximately 2.7×10^{-3}, suggesting only moderate structural reorganization in the excited state.

To evaluate the CPL-emitting performance of **4g**, its CPL brightness (B_{CPL}) was determined using equation [53, 54],

$$B_{CPL} = g_{lum} \cdot \Phi_{fl} \cdot \varepsilon/2$$

where Φ_{fl} is the fluorescence quantum yield and ε is the molar absorptivity at a fixed wavelength, typically the absorption maximum. The B_{CPL} value obtained for dye **4g** in dichloromethane is 17.2 M^{-1} cm^{-1} (Table 2), which classifies this compound as a moderate-to-good CPL emitter [53–55]. Additional chiroptical measurements of **4g** were performed in hexane to assess the effect of solvent polarity (Figure S48). The g_{lum} value, approximately 2.0×10^{-3}, is very similar to that measured in dichloromethane and closely matches the g_{abs} value of the lowest-energy absorption band (Figure S49). The corresponding CPL brightness is 12.5 M^{-1} cm^{-1} (Table 2). To assign the absolute configuration of each eluted fraction of **4g**, TD-DFT calculations were performed according to the procedure detailed in the Supporting Information. Comparison of the calculated and experimental CD spectra shown in Figure S48, particularly the signs of the main bands, enabled assignment of the absolute configuration. Specifically, the second eluted fraction of **4g** was assigned to the (*M,M*) enantiomer.

2.3 | First-Principles Calculations

To probe the nature of the excited states involved in the synthesized compounds and how they are affected by substitution, we performed first-principles calculations using a protocol previously applied to DHPPs by our groups [55–57]. In this protocol, the ground- and excited-state structures were determined using DFT and TD-DFT, respectively, whereas total and transition energies were calculated at the second-order coupled-cluster level (CC2), and solvent effects, here toluene, were modeled using the cLR^2-PCM solvation approach [57, 58]. Details of this protocol are provided in the Supporting Information. The main results are summarized in Table 3.

For all compounds studied here, both C_2 and C_i point-group structures can be considered, depending on the relative orientations of the substituents around the DHPP core. We optimized all structures in both symmetries (Figures S54–S69). For most dyes, the two point groups give optimized geometries with similar energies, with differences below 2 kcal mol^{-1}, suggesting that both forms may coexist in solution. However, for **4a** and **4g**, the bowl-shaped C_2 structures are markedly more stable.

For dye **4a**, the excited-state structures are stable in both point groups, as confirmed by the absence of imaginary frequencies, and theory predicts a 0–0 energy of 2.74 eV for the most stable C_2 conformer, in reasonable agreement with the experimental absorption/emission crossing point at 2.92 eV. The electron-density-difference (EDD) plots corresponding to this transition are shown in Figure 4. As expected, the transition has a rather localized π–π^* character, centered on the DHPP core, consistent with the absence of any significant solvatochromic or solvatofluorochromic effect in the experiment. For this compound, we simulated the vibronic profiles of both absorption and fluorescence for both point groups (see Figures S71–S72). These computations successfully reproduce the experimental absorption and emission band shapes, including all key features. For the C_2 conformer, the three main peaks are accurately reproduced, together with their relative broadening. In contrast, the spectrum calculated for the C_i conformer shows the three main peaks blue-shifted by approximately 20 nm and exhibits a more pronounced fine structure than that of the C_2 conformer, particularly for the first two peaks, which appear too narrow relative to the experimental data. The computed molar absorption coefficient for the most intense band is approximately 50 000 M^{-1} cm^{-1} for both point groups, in good agreement with the experimental values. Regarding emission, both the C_2 and C_i spectra successfully reproduce the fine structure of the two main peaks. However, as observed for the absorption spectra, the C_i emission is blue-shifted by approximately 30 nm. The better agreement obtained for the C_2 spectra, together with the relative ground-state energies estimated previously (Table 3), supports the assignment of a C_2 geometry for **4a** in solution at room temperature.

For **4b** and **4f**, both conformations are likely to coexist in solution (Figures S56–S67). Theory predicts rather similar absorption and emission energies for the two conformers, although the C_i conformer undergoes slight excited-state symmetry breaking for **4b** and **4f**, even in toluene. This result is consistent with the experimental observation of limited solvatochromism but more pronounced solvatofluorochromism for these two compounds. Indeed, the EDD plots suggest that a significant quadrupolar charge-transfer character appears in both **4b** and **4f**, with DHPP acting as an electron-donating moiety and the peripheral aromatic rings acting as accepting units. We note that the evolution of the absorption and emission wavelengths predicted by theory, relative to **4a**, matches the experimental trends well, especially when considering the most stable conformers for each dye. In the nitro-substituted dyes **4c** and **4d**, the charge-transfer character is pronounced, and the nitro groups, which are slightly twisted relative to the adjacent six-membered rings because of steric hindrance, act as electron acceptors, as expected (Figure 4). This enhanced charge-transfer character leads to excited-state symmetry breaking and strongly red-shifted fluorescence, especially for **4d**, in agreement with both theory and experiment. Dye **4e** behaves similarly, although the charge-transfer character is less pronounced than in the nitro-substituted compounds, consistent

21951071, 2026, 39, Downloaded from https://advanced.onlinelibrary.wiley.com/doi/10.1002/adom.71894 by Francesca Terenziani - University Degli Studi Di Parma Stampa Universitaria Parmense , Wiley Online Library on [26/10/2026]. See the Terms and Conditions (https://onlinelibrary.wiley.com/terms-and-conditions) on Wiley Online Library for rules of use; OA articles are governed by the applicable Creative Commons License

TABLE 3 | Computational results for dyes **4a-4g**.

	S_0 PG	ΔE (kcal/mol)	$\lambda^{vert-abs}$ (nm)	S_1 PG	$\lambda^{vert-fl}$ (nm)	ΔE^{0-0} (eV)
4a	C_2	0.00	386	C_2	441	2.74
	C_i	6.15	381	C_i	428	2.78
4b	C_2	0.45	403	C_2	468	2.55
	C_i	0.00	397	C_1	467	2.70
4c	C_2	0.00	424	C_1 [a]	574[a]	2.09
	C_i	1.29	421	C_1 [a]	574[a]	2.02
4d	C_2	0.00	397	C_1	617	2.08
	C_i	1.19	407	C_1	631	2.04
4e	C_2	0.00	430	C_1	[b]	[b]
	C_i	0.62	432	C_1	519	2.30
4f	C_2	0.70	385	C_1	431	2.81
	C_i	0.00	386	C_1	446	2.73
4g	C_2	0.00	444	C_2	491	2.35
	C_i	5.22	437	C_1	518	2.49

PG – conformers' point group and ΔE their relative ground-state energies (PCM-DFT, *E*+ZPVE), $\lambda^{vert-abs}$ / $\lambda^{vert-fl}$ – vertical absorption / emission wavelengths, ΔE^{0-0} – 0-0 transition energies. All the latter are CC2-corrected.

[a]in **4c**, the excited-state optimization starting from the C_2 and C_i ground-state structures yields imaginary frequencies. Lowering the structures to C_1 delivers the same optimal structure for the two starting points

[b]the CC2 calculation did not converge in that case.

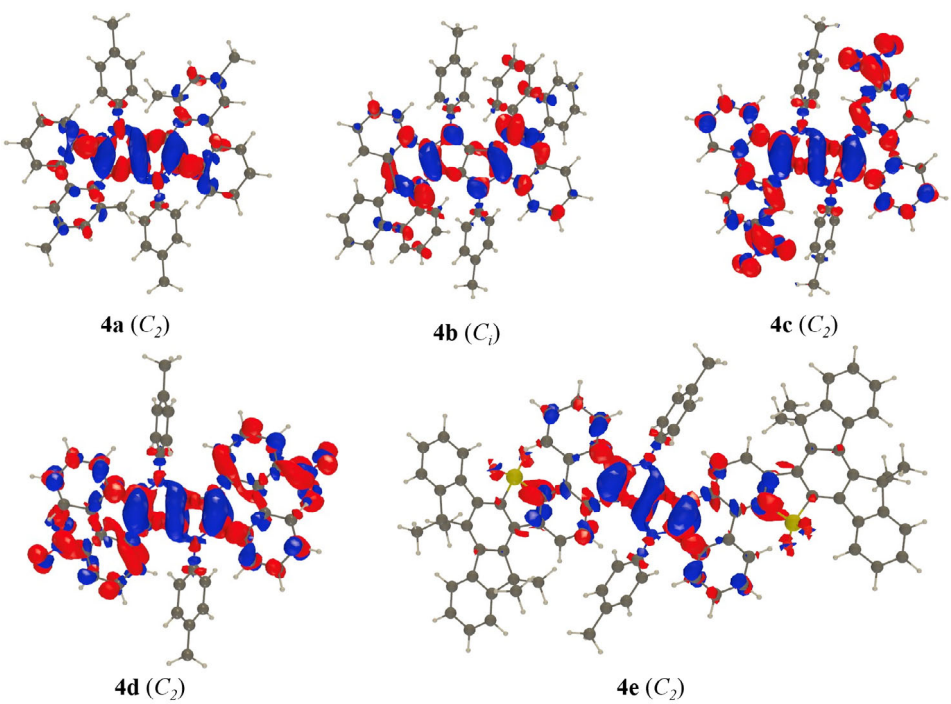


FIGURE 4 | Electron density difference (EDD) plots corresponding to the absorption to the lowest state of selected compounds. The blue and red lobes represent regions of decrease and increase of electron density (threshold: 0.001 au). Complete data are provided in the SI.

with the weaker experimental solvatochromism observed for **4e** compared with **4c** and **4d**.

Finally, in **4g**, the more stable C_2 conformer has a highly delocalized excited state, but with a less pronounced charge-transfer character (Figures S6 and S68). Theory does not predict excited-state symmetry breaking in this case, but does predict red-shifted absorption and emission relative to **4a**, in excellent agreement with the experimental measurements. Overall, these theoretical results confirm that subtle struc-

21951071, 2026, 39, Downloaded from https://advanced.onlinelibrary.wiley.com/doi/10.1002/adom.71894 by Francesca Terenziani - University Degli Studi Di Parma Stampa Universitaria Parmense , Wiley Online Library on [26/10/2026]. See the Terms and Conditions (https://onlinelibrary.wiley.com/terms-and-conditions) on Wiley Online Library for rules of use; OA articles are governed by the applicable Creative Commons License

tural changes give rise to a broad range of photophysical behaviors.

2.4 | Electrochemistry

To evaluate the electrochemical properties of the synthesized compounds, cyclic voltammograms were recorded in 1,2-dichlorobenzene containing 0.1 M (TBA)PF_6 as the supporting electrolyte (Figures S50, S51, S52 and S53). Owing to the electron-rich nature of the DHPP core, all systems exhibit a quasi-reversible redox process, indicating the formation of a relatively stable radical cation. The presence of electron-withdrawing substituents modulates the oxidation potential, leading to a shift of the first oxidation potential from 0.077 V vs Fc/Fc^+ for **4a** to 0.458 V vs Fc/Fc^+ for **4d** (Table S3). Further oxidations are generally irreversible and lead to adsorption of decomposition products on the electrode surface. Notably, the electrochemical response of **4g**, which possesses a more complex three-dimensional structure, is richer than those of the other investigated dyes, displaying a larger number of oxidation processes (Figure S50 and S52).

In contrast, neither **4b** nor **4g** exhibits reduction processes within the accessible negative potential window, whereas irreversible reduction processes are observed for **4a** and **4c–f** between −0.9 and −1.5 V vs Fc/Fc^+ (Table S3, Figure S51). Compared with the other systems, the nitro-substituted dyes **4c** and **4d** show more complex reduction behavior, with multiple overlapping processes. This likely results from reduction of both the π-electron system and the nitro groups themselves.

3 | Conclusions

In summary, we have developed a facile and modular synthetic strategy for the construction of structurally diverse, π-expanded DHPPs. The key advantage of this strategy over previously reported approaches is its broad substrate scope. This approach relies on double intramolecular direct arylation, providing a robust strategy that tolerates significant steric demand and electron-deficient substituents, thereby enabling the synthesis of large molecular frameworks. As a result of this strategy being compatible with various electronic and steric factors, the photophysical properties of these dyes can be systematically modulated, e.g., with emission extending beyond 700 nm.

This robust protocol provides access to diverse architectures, ranging from π-expanded DHPPs containing up to 20 fused rings to a helically twisted B, N-doped system, whose enantiomers could be resolved and characterized chiroptically. The latter exhibits measurable CPL activity, with a CPL brightness reaching approximately 17 M^{-1} cm^{-1}. Theoretical analysis demonstrated that the central DHPP unit consistently acts as the main electron-donating moiety, whereas the nature and position of the peripheral groups enable extensive tuning of the optical properties. Overall, this synthetic platform opens the door to scalable and cost-effective access to functional N-doped nanographenes and offers considerable potential for the future development of optoelectronic materials.

4 | Experimental Section

4.1 | Synthesis

All reagents and solvents were purchased from commercial sources and were used as received unless otherwise noted. For water-sensitive reactions, solvents were dried using a Solvent Purification System from MBraun (https://www.mbraun.com/us/). Reactions involving moisture- and oxygen-sensitive compounds were performed under a stream of argon. The reaction progress was monitored by means of thin-layer chromatography (TLC), which was performed on aluminium foil plates, covered with Silica gel 60 F254 (Merck). Product purification was done by means of column chromatography with Kieselgel 60 (200-400 mesh, Merck).

The identity and purity of the prepared compounds were proved by ^{1}H NMR and ^{13}C NMR spectrometry as well as by MS spectrometry (via EI-MS, ESI-MS or APCI-MS). NMR spectra were measured on Bruker AM 500 MHz, Varian 600 MHz, and Varian 500 MHz instruments with TMS as the internal standard. Chemical shifts for ^{1}H NMR are expressed in parts per million (ppm) relative to tetramethylsilane (δ 0.00 ppm), $CDCl_3$ ($\delta = 7.26$ ppm), CD_2Cl_2 ($\delta = 5.33$ ppm), DMSO-d6 ($\delta = 2.50$ ppm). Chemical shifts for ^{13}C NMR are expressed in ppm relative to $CDCl_3$ (δ 77.16 ppm), CD_2Cl_2 (53.84 ppm), DMSO-d6 (δ = 39.52 ppm). Data are reported as follows: chemical shift, multiplicity (s = singlet, bs = broad singlet, d = doublet, dd = doublet of doublets, ddd = doublet of doublet of doublets, t = triplet, td = triplet of doublets, q = quartet, qu = quintet, m = multiplet), coupling constant (Hz), and integration.

Author Contributions

Damian Kusy: conceptualization, visualization, Writing – original draft, investigation, Writing – review and editing. **Krzysztof Górski**: writing – original draft, writing – review and editing. **Carmelo Naim**: investigation, visualization, writing – original draft. **Francesco Bertocchi**: investigation, visualization. **Nicolas Vanthuyne**: investigation, visualization. **Krzysztof Noworyta**: investigation, visualization. **Bartosz Szymański**: investigation, visualization. **Radosław Kamiński**: supervision. **Francesca Terenziani**: investigation, supervision, writing – original draft. **Denis Jacquemin**: supervision, writing – original draft, writing – review and editing, funding acquisition. **Daniel T. Gryko**: conceptualization, writing – original draft, writing – review and editing, project administration, funding acquisition.

Acknowledgements

This work was supported by the Polish National Science Center, Poland (grants OPUS 2020/37/B/ST4/00017). This project has received funding from the European Research Council (ARCHIMEDES, 101097337). Views and opinions expressed are, however, those of the authors only and do not necessarily reflect those of the European Union or the European Research Council Executive Agency. Neither the European Union nor the granting authority can be held responsible for them. The collaboration between the Jacquemin's and Gryko's groups is supported by the Maria Skłodowska-Curie and Pierre Curie Polish-French Science Award of the Académie des Sciences, the FNP and Zygmunt Zaleski foundation. This work used the HPC resources from the GLiCID Computing Facility (Ligerien Group for Intensive Distributed Computing, 10.60487/glicid, Pays de la Loire, France).

21951071, 2026, 39, Downloaded from https://advanced.onlinelibrary.wiley.com/doi/10.1002/adom.71894 by Francesca Terenziani - University Degli Studi Di Parma Stampa Universitaria Parmense , Wiley Online Library on [26/10/2026]. See the Terms and Conditions (https://onlinelibrary.wiley.com/terms-and-conditions) on Wiley Online Library for rules of use; OA articles are governed by the applicable Creative Commons License

Open access publishing facilitated by Universita degli Studi di Parma, as part of the Wiley - CRUI-CARE agreement.

Conflicts of Interest

The authors declare no conflicts of interest.

Data Availability Statement

The data that supports the findings of this study are available in the supplementary material of this article.

References

1. M. Żyła, E. Gońka, P. J. Chmielewski, J. Cybińska, and M. Stępień, "Synthesis of a Peripherally Conjugated 5-6-7 Nanographene," *Chemical Science* 7 (2016): 286–294.

2. E. Jin, Q. Yang, C.-W. Ju, et al., "A Highly Luminescent Nitrogen-Doped Nanographene as an Acid- and Metal-Sensitive Fluorophore for Optical Imaging," *Journal of the American Chemical Society* 143, no. 27 (2021): 10403–10412.

3. H. Yokoi, Y. Hiraoka, S. Hiroto, D. Sakamaki, S. Seki, and H. Shinokubo, "Nitrogen-Embedded Buckybowl and Its Assembly with C60," *Nature Communications* 6, no. 1 (2015): 8215.

4. Z. Qiu, X. Chen, Y. Huang, et al., "Nanographene with Multiple Embedded Heptagons: Cascade Radical Photocyclization," *Angewandte Chemie International Edition* 61 (2022): e202116955, https://doi.org/10.1002/anie.202116955.

5. S. Hayakawa, A. Kawasaki, Y. Hong, et al., "Inserting Nitrogen: An Effective Concept To Create Nonplanar and Stimuli-Responsive Perylene Bisimide Analogues," *Journal of the American Chemical Society* 141, no. 50 (2019): 19807–19816.

6. F. Chen, Y. S. Hong, S. Shimizu, D. Kim, T. Tanaka, and A. Osuka, "Synthesis of a Tetrabenzotetraaza[8]Circulene by a 'Fold-In' Oxidative Fusion Reaction," *Angewandte Chemie* 127 (2015): 10785–10788.

7. Y. Matsuo, M. Gon, K. Tanaka, S. Seki, and T. Tanaka, "Benzannulated Double Aza[9]Helicenes: Synthesis, Structures, and (Chir)Optical Properties," *Chemistry – An Asian Journal* 19 (2024): e202400134, https://doi.org/10.1002/asia.202400134.

8. W. Zhang, Y. Ding, S. Yu, et al., "Highly Strained Electron-Rich Molecular Bowl and Nanographene," *Angewandte Chemie International Edition* 64 (2025): 1–7.

9. R. E. Messersmith, M. A. Siegler, and J. D. Tovar, "Aromaticity Competition in Differentially Fused Borepin-Containing Polycyclic Aromatics," *The Journal of Organic Chemistry* 81, no. 13 (2016): 5595–5605.

10. K. Bartkowski and M. Pawlicki, "(Aza)Acenes Share the C2 Bridge with (Anti)Aromatic Macrocycles: Local vs. Global Delocalization Paths," *Angewandte Chemie International Edition* 60, no. 16 (2021): 9063–9070.

11. M. Stępień, E. Gońka, M. Żyła, and N. Sprutta, "Heterocyclic Nanographenes and Other Polycyclic Heteroaromatic Compounds: Synthetic Routes, Properties, and Applications," *Chemical Reviews* 117 (2017): 3479–3716.

12. A. Borissov, Y. K. Maurya, L. Moshniaha, W.-S. Wong, M. Żyła-Karwowska, and M. Stępień, "Recent Advances in Heterocyclic Nanographenes and Other Polycyclic Heteroaromatic Compounds," *Chemical Reviews* 122, no. 1 (2022): 565–788.

13. S. Ito, Y. Tokimaru, and K. Nozaki, "Benzene-Fused Azacorannulene Bearing an Internal Nitrogen Atom," *Angewandte Chemie International Edition* 54, no. 25 (2015): 7256–7260.

14. K. Oki, M. Takase, S. Mori, et al., "Synthesis, Structures, and Properties of Core-Expanded Azacoronene Analogue: A Twisted π-System with Two N-Doped Heptagons," *Journal of the American Chemical Society* 140, no. 33 (2018): 10430–10434.

15. J. Wagner, P. Zimmermann Crocomo, M. A. Kochman, A. Kubas, P. Data, and M. Lindner, "Modular Nitrogen-Doped Concave Polycyclic Aromatic Hydrocarbons for High-Performance Organic Light-Emitting Diodes with Tunable Emission Mechanisms," *Angewandte Chemie International Edition* 61 (2022): e202202232, https://doi.org/10.1002/anie.202202232.

16. Y. S. Park, D. J. Dibble, J. Kim, R. C. Lopez, E. Vargas, and A. A. Gorodetsky, "Synthesis of Nitrogen-Containing Rubicene and Tetrabenzopentacene Derivatives," *Angewandte Chemie International Edition* 55 (2016): 3352–3355.

17. U. H. F. Bunz, "The Larger Linear N-Heteroacenes," *Accounts of Chemical Research* 48, no. 6 (2015): 1676–1686.

18. B. Yang, Y. Sun, J. Hu, et al., "Triazasupersumanenes: Bowl-Shaped Nanographenes with Tunable Properties and Unexpected Charge Transport Performance," *Chem* 11 (2025): 102628, https://doi.org/10.1016/j.chempr.2025.102628.

19. J. Fan, L. Zhang, A. L. Briseno, and F. Wudl, "Synthesis and Characterization of 7,8,15,16-Tetraazaterrylene," *Organic Letters* 14 (2012): 1024–1026.

20. K. Oki, M. Takase, S. Mori, and H. Uno, "Synthesis and Isolation of Antiaromatic Expanded Azacoronene via Intramolecular Vilsmeier-Type Reaction," *Journal of the American Chemical Society* 141, no. 41 (2019): 16255–16259.

21. H. Kitano, W. Matsuoka, H. Ito, and K. Itami, "Annulative π-Extension of Indoles and Pyrroles with Diiodobiaryls by Pd Catalysis: Rapid Synthesis of Nitrogen-Containing Polycyclic Aromatic Compounds," *Chemical Science* 9, no. 38 (2018): 7556–7561.

22. D. Myśliwiec and M. Stępień, "The Fold-In Approach to Bowl-Shaped Aromatic Compounds: Synthesis of Chrysaoroles," *Angewandte Chemie* 125 (2013): 1757–1761.

23. C. L. Anderson, T. Zhang, M. Qi, et al., "Exceptional Electron-Rich Heteroaromatic Pentacycle for Ultralow Band Gap Conjugated Polymers and Photothermal Therapy," *Journal of the American Chemical Society* 145, no. 9 (2023): 5474–5485.

24. F. Gan, C. Shen, W. Cui, and H. Qiu, "[1,4]Diazocine-Embedded Electron-Rich Nanographenes with Cooperatively Dynamic Skeletons," *Journal of the American Chemical Society* 145, no. 10 (2023): 5952–5959.

25. M. Krzeszewski, D. Gryko, and D. T. Gryko, "The Tetraarylpyrrolo[3,2-b]Pyrroles – From Serendipitous Discovery to Promising Heterocyclic Optoelectronic Materials," *Accounts of Chemical Research* 50 (2017): 2334–2345.

26. M. Krzeszewski, K. Sahara, Y. M. Poronik, T. Kubo, and D. T. Gryko, "Unforeseen 1,2-Aryl Shift in Tetraarylpyrrolo[3,2- b]Pyrroles Triggered by Oxidative Aromatic Coupling," *Organic Letters* 20, no. 6 (2018): 1517–1520.

27. G. Sanil, M. Krzeszewski, W. Chaładaj, et al., "Gold-Catalyzed 1,2-Aryl Shift and Double Alkyne Benzannulation," *Angewandte Chemie International Edition* 62, no. 49 (2023): 1–9.

28. G. Sanil, Ł. Dobrzycki, M. K. Cyrański, D. Jacquemin, W. Chaładaj, and D. T. Gryko, "1,4-Dihydropyrrolo[3,2- b]Pyrroles with Two Embedded Heptagons via Alkyne Annulation," *The Journal of Organic Chemistry* 90 (2025): 614–622.

29. K. Górski, S. Shelton, J. Lingagouder, P. Data, D. Jacquemin, and D. T. Gryko, "1,4-Dihydropyrrolo[3,2- b]Pyrrole Modified with Dibenzoxazepine: A Highly Efficient Core for Charge-Transfer-Based OLED Emitters," *Chemical Science* 16 (2025): 5223–5233.

30. P. P. Abatti, N. O. Decarli, S. Gogoc, et al., "Shedding Light on Highly Emissive 1,4-Dihydropyrrolo[3,2-b]Pyrrole Derivatives: Synthesis and Aggregate-Dependent Emission," *ChemPlusChem* 88 (2023): 202300539.

31. K. Górski, Ł. W. Ciszewski, A. Wrzosek, A. Szewczyk, A. L. Sobolewski, and D. T. Gryko, "An Efficient Method for the Synthesis of π-Expanded Phosphonium Salts," *Organic Chemistry Frontiers* 12 (2025): 5484–5495.

21951071, 2026, 39, Downloaded from https://advanced.onlinelibrary.wiley.com/doi/10.1002/adom.71894 by Francesca Terenziani - University Degli Studi Di Parma Stampa Universitaria Parmense , Wiley Online Library on [26/10/2026]. See the Terms and Conditions (https://onlinelibrary.wiley.com/terms-and-conditions) on Wiley Online Library for rules of use; OA articles are governed by the applicable Creative Commons License

32. V. G. More, R. W. Jadhav, M. Al Kobaisi, L. A. Jones, and S. V. Bhosale, *Handb. Aggregation-Induced Emiss*, (Wiley, 2022), 221–253.

33. G. S. Collier, "Dihydropyrrolo[3,2- b]Pyrroles as Novel Conjugated Polymers: Leveraging Simplicity for Sustainability and Student Success," *Accounts of Chemical Research* 59, no. 13 (2026): 2170–2181, https://doi.org/10.1021/acs.accounts.6c00298.

34. M. Krzeszewski and D. T. Gryko, "χ-Shaped Bis(areno)-1,4-dihydropyrrolo[3,2- b]Pyrroles Generated by Oxidative Aromatic Coupling," *The Journal of Organic Chemistry* 80, no. 5 (2015): 2893–2899.

35. M. Krzeszewski, P. Świder, Ł. Dobrzycki, M. K. Cyrański, W. Danikiewicz, and D. T. Gryko, "The Role of Steric Hindrance in the Intramolecular Oxidative Aromatic Coupling of Pyrrolo[3,2-b]Pyrroles," *Chemical Communications* 52, no. 77 (2016): 11539–11542.

36. D. T. Gryko, V. I. Vullev, and T. Kubo, "Nonplanar Butterfly-Shaped p-Expanded Pyrrolopyrroles Supporting Information," *Chemistry – A European Journal* 2 (2016): 1–5.

37. M. Krzeszewski, Ł. Dobrzycki, A. L. Sobolewski, M. K. Cyrański, and D. T. Gryko, "Bowl-Shaped Pentagon- and Heptagon-Embedded Nanographene Containing a Central Pyrrolo[3,2- b]Pyrrole Core," *Angewandte Chemie International Edition* 60, no. 27 (2021): 14998–15005.

38. M. Krzeszewski, Ł. Dobrzycki, A. L. Sobolewski, M. K. Cyrański, and D. T. Gryko, "Saddle-Shaped Aza-Nanographene with Multiple Odd-Membered Rings," *Chemical Science* 14, no. 9 (2023): 2353–2360.

39. S. Mishra, M. Krzeszewski, C. A. Pignedoli, P. Ruffieux, R. Fasel, and D. T. Gryko, "On-Surface Synthesis of a Nitrogen-Embedded Buckybowl with Inverse Stone–Thrower–Wales Topology," *Nature Communications* 9 (2018): 1714.

40. M. B. Teimouri, I. Deperasińska, M. Rammo, et al., "Strongly Polarized π-Extended 1,4-Dihydropyrrolo[3,2- b]Pyrroles Fused with Tetrazolo[1,5-a]Quinolines," *The Journal of Organic Chemistry* 89, no. 7 (2024): 4657–4672.

41. K. Górski, L. Pejov, K. B. Jørgensen, I. Knysh, D. Jacquemin, and D. T. Gryko, "Twofold 6π-Electrocyclization as a Route toward Multi-Heteroatom-Doped Nanographenes Built on a 1,4-Dihydropyrrolo[3,2-b]Pyrrole Core" *Chemistry – A European Journal* 31 (2024): 202404094, https://doi.org/10.1002/chem.202404094.

42. D. Kusy, K. Górski, F. Bertocchi, et al., "Synthesis and Chiroptical Activity of π-Expanded Electron-Rich Heterohelicenes Based on the 1,4-Dihydropyrrolo[3,2- b]Pyrrole Core," *Chemistry – A European Journal* 31 (2025): e202404632, https://doi.org/10.1002/chem.202404632.

43. M. S. Molloy, J. A. Snyder, J. R. DeFrancisco, and A. E. Bragg, "Structural Control of Nonadiabatic Photochemical Bond Formation: Photocyclization in Structurally Modified Orth o -Terphenyls," *The Journal of Physical Chemistry A* 120, no. 23 (2016): 3998–4007.

44. K. J. Kochanowski, K. Górski, D. Kusy, et al., "Synthesis and Chiral Optical Activity of a Quadruple Heterohelicene Based on 1,4-dihydropyrrolo[3,2-b]Pyrrole–picene Hybrid," *Journal of Materials Chemistry C* 14 (2026): 6692–6699.

45. M. Tasior, O. Vakuliuk, D. Koga, et al., "Method for the Large-Scale Synthesis of Multifunctional 1,4-Dihydro-pyrrolo[3,2- b]Pyrroles," *The Journal of Organic Chemistry* 85, no. 21 (2020): 13529–13543.

46. F. Terenziani, A. Painelli, C. Katan, M. Charlot, and M. Blanchard-Desce, "Charge Instability in Quadrupolar Chromophores: Symmetry Breaking and Solvatochromism," *Journal of the American Chemical Society* 128, no. 49 (2006): 15742–15755.

47. B. Dereka, A. Rosspeintner, Z. Li, R. Liska, and E. Vauthey, "Direct Visualization of Excited-State Symmetry Breaking Using Ultrafast Time-Resolved Infrared Spectroscopy," *Journal of the American Chemical Society* 138, no. 13 (2016): 4643–4649.

48. K. Górski, K. Noworyta, and J. Mech-Piskorz, "Influence of the Heteroatom Introduction on the Physicochemical Properties of 5-Heterotruxenes Containing Nitrogen, Oxygen and Sulfur Atom," *RSC Advances* 10 (2020): 42363–42377.

49. Y. M. Poronik, G. V. Baryshnikov, I. Deperasińska, et al., "Deciphering the Unusual Fluorescence in Weakly Coupled Bis-nitro-pyrrolo[3,2-b]Pyrroles," *Communications Chemistry* 3, no. 1 (2020): 190.

50. Ł. G. Łukasiewicz, H. G. Ryu, A. Mikhaylov, et al., "Symmetry Breaking in Pyrrolo[3,2- b]Pyrroles: Synthesis, Solvatofluorochromism and Two-Photon Absorption," *Chemistry – An Asian Journal* 12 (2017): 1736–1748.

51. R. Englman and J. Jortner, "The Energy Gap Law for Radiationless Transitions in Large Molecules," *Molecular Physics* 18, no. 2 (1970): 145–164.

52. G. Longhi, E. Castiglioni, J. Koshoubu, G. Mazzeo, and S. Abbate, "Circularly Polarized Luminescence: A Review of Experimental and Theoretical Aspects," *Chirality* 28, no. 10 (2016): 696–707.

53. W. D. Petrykowski, N. Vanthuyne, C. Naim, et al., "Double Helicene Possessing B–N Dative Bonds Built on 1,4-dihydropyrrolo[3,2- b]Pyrrole Core," *Chemical Science* 16 (2025): 8338–8345.

54. L. Arrico, L. Di Bari, and F. Zinna, "Quantifying the Overall Efficiency of Circularly Polarized Emitters," *Chemistry – A European Journal* 27 (2021): 2920–2934.

55. M. Cei, L. Di Bari, and F. Zinna, "Circularly Polarized Luminescence of Helicenes: A Data-Informed Insight," *Chirality* 35, no. 4 (2023): 192–210.

56. M. Tasior, B. Koszarna, D. C. Young, et al., "Fe(iii)-Catalyzed Synthesis of Pyrrolo[3,2- b]Pyrroles: Formation of New Dyes and Photophysical Studies," *Organic Chemistry Frontiers* 6, no. 16 (2019): 2939–2948.

57. Y. M. Poronik, L. M. Mazur, M. Samoć, D. Jacquemin, and D. T. Gryko, "2,5-Bis(azulenyl)Pyrrolo[3,2-b]Pyrroles – the Key Influence of the Linkage Position on the Linear and Nonlinear Optical Properties," *Journal of Materials Chemistry C* 5 (2017): 2620–2628.

58. C. A. Guido, A. Chrayteh, G. Scalmani, B. Mennucci, and D. Jacquemin, "Simple Protocol for Capturing both Linear-Response and State-Specific Effects in Excited-State Calculations with Continuum Solvation Models," *Journal of Chemical Theory and Computation* 17, no. 8 (2021): 5155–5164.

Supporting Information

Additional supporting information can be found online in the Supporting Information section.

Supporting File: adom71894-sup-0001-SuppMat.docx.

21951071, 2026, 39, Downloaded from https://advanced.onlinelibrary.wiley.com/doi/10.1002/adom.71894 by Francesca Terenziani - University Degli Studi Di Parma Stampa Universitaria Parmense , Wiley Online Library on [26/10/2026]. See the Terms and Conditions (https://onlinelibrary.wiley.com/terms-and-conditions) on Wiley Online Library for rules of use; OA articles are governed by the applicable Creative Commons License